Raman spectroscopy determination of the Debye temperature and atomic cohesive energy of CdS, CdSe, Bi2Se3, and Sb2Te3 nanostructures

Zhou, Zhaofeng; Sun, Changqing; Yang, X. X.; Wang, Y.; Jiang, R.; Zheng, W. T.

2012

Yang, X. X., Zhou, Z. F., Wang, Y., Jiang, R., Zheng, W. T., & Sun, C. Q. (2012). Raman spectroscopy determination of the Debye temperature and atomic cohesive energy of CdS, CdSe, Bi2Se3, and Sb2Te3 nanostructures. Journal of Applied Physics, 112(8), 083508.

https://hdl.handle.net/10356/95444

https://doi.org/10.1063/1.4759207

AIP | Journal of Applied Physics

Raman spectroscopy determination of the Debye temperature and atomic cohesive energy of CdS, CdSe, Bi2Se3, and Sb2Te3 nanostructures

X. X. Yang, Z. F. Zhou, Y. Wang, R. Jiang, W. T. Zheng et al.

Citation: J. Appl. Phys. **112**, 083508 (2012); doi: 10.1063/1.4759207
View online: http://dx.doi.org/10.1063/1.4759207
View Table of Contents: http://jap.aip.org/resource/1/JAPIAU/v112/i8
Published by the American Institute of Physics.

Raman spectroscopy determination of the Debye temperature and atomic cohesive energy of CdS, CdSe, Bi_2Se_3, and Sb_2Te_3 nanostructures

X. X. Yang,[1] Z. F. Zhou,[1,a)] Y. Wang,[2] R. Jiang,[1] W. T. Zheng,[3] and Chang Q. Sun[4,a)]
[1]*Key Laboratory of Low-Dimensional Materials and Application Technologies, Institute for Quantum Engineering and Micro-Nano Energy Technology, Faculty of Materials, Optoelectronic and Physics, Xiangtan University, Hunan 411105, China*
[2]*School of Information and Electronic Engineering, Hunan University of Science and Technology, Xiangtan 411201, China*
[3]*School of Materials Science, Jilin University, Changchun 130012, China*
[4]*School of Electrical and Electronic Engineering, Nanyang Technological University, Singapore 639798*

(Received 27 June 2012; accepted 19 September 2012; published online 18 October 2012)

We have formulated the size and temperature dependence of the phonon relaxation dynamics for CdS, CdSe, Bi_2Se_3, and Sb_2Te_3 nanostructures based on the framework of bond order–length–strength correlation, core-shell configuration, and local bond averaging approach. The Raman shifts are correlated directly to the identities (nature, order, length, and energy) of the representative bond of the specimen without needing involvement of the Grüneisen mode parameters or considering the processes of phonon decay or multi-phonon resonant scattering. Quantitative information of the Debye temperature, the atomic cohesive energy, the reference frequencies from which the Raman shifts proceed, and the effective coordination numbers of the randomly sized particles, as well as the length and energy of the representative bond, has been obtained. It is clarified that the size-induced phonon softening arises intrinsically from the cohesive weakening of the undercoordinated atoms in the skin up to three atomic layers and the thermally derived phonon softening results from the thermally lengthening and weakening of bonds. Developed approach empowers the Raman technique in deriving quantitative and direct information regarding bond stiffness relaxation with applied stimuli such as coordination, mechanical, thermal, and chemical environment, which are crucial to practical applications. [http://dx.doi.org/10.1063/1.4759207]

I. INTRODUCTION

Compound semiconductors such as CdS, CdSe, Bi_2Se_3, and Sb_2Te_3 are of technological importance in various scientific and technological branches. These semiconductors have widely been used in field effect transistors,[1–3] infrared-THz detectors,[4,5] magnetic sensors,[6,7] and devices involving electron-phonon coupling, photoabsorption, and photoemission in carrier transportation.[8–10] Overwhelming contributions have been made to explore the phonon dynamics in terms of Raman shifts under various conditions such as changing particle size[11–14] and varying operating temperature.[15–18]

Generally, a red-shift of Raman optical phonons occurs when the solid size is reduced. The size-induced phonon red shift has been suggested to be activated by surface disorder,[19] surface stress,[20–22] and phonon quantum confinement.[23,24] The phonon confinement model[24] suggested that strong phonon damping happens with decreasing solid size, whereas correlation function calculations[25] argued that the phonon softening arises from the drop of local dielectric constant, instead of phonon damping.

When the specimen is being heated, the Raman phonons also undergo a red shift. Traditionally, phonon dispersions and their concomitant anharmonic effects are described in terms of mode Grüneisen parameters $\gamma = -\partial\omega/\partial V$ or $\gamma_E = -\partial Ln\omega/\partial LnV$. The mode Grüneisen parameters have also been employed to describe the strain effect on the change of volume.[26] Anharmonic coupling for multi-phonon decay channels[16] are also involved with derivative of information regarding the correlation between the Raman shift and temperature without intrinsic information being derived.

Currently available models for the optical phonon softening are based on assumptions that the materials are homogeneous and isotropic, which is valid only in the long-wavelength limit. When the size of the solid is in the nanometer range, the continuum dielectric models become invalid. Therefore, deeper insight into the physical origin of the size- and temperature-induced red shift is highly desirable. Furthermore, the sophisticated Raman measurements challenge for more useful information than insofar one can obtain.[27,28]

The objective of this work is to show that our original set of the bond-order–length–strength (BOLS) correlation mechanism,[29] the core-shell configuration, and the local bond averaging (LBA) approach[30] has enabled us to reproduce the size and temperature trends of Raman shifts with clarification of their physical origin of the vibration frequency shift. Reproduction of the observations revealed that the size-induced softening of CdS, CdSe, and Bi_2Se_3 nanostructures arises from the cohesive weakening of the

a)Authors to whom correspondence should be addressed. Electronic addresses: zfzhou@xtu.edu.cn and ecqsun@ntu.edu.sg.

undercoordinated atoms in the skin of a nanosolid and the thermal-softening of CdS, Bi_2Se_3, and Sb_2Te_3 phonons as arises intrinsically from the thermal lengthening and weakening of the involved bonds. This set of approaches has also enabled us to gain quantitative information of the atomic cohesive energy $E_B(0)$, the effective coordination numbers (CNs) for the randomly sized particles, and the Debye temperature as well as the reference frequency $\omega(1)$ from which the Raman shift proceeds.

II. THEORY

A. The Raman shift

Instead of the Raman phonon decaying or scattering, we emphasize that the solution to the Hamiltonian of a vibration system is a Fourier series with multiple terms of frequencies being folds of that of the primary mode.[31] Generally, one can measure the Raman resonance frequency as $\omega = \omega_0 + \Delta\omega$, where ω_0 is the reference point from which the Raman shift $\Delta\omega$ proceeds under the applied stimuli. The ω_0 may vary with the frequency of the incident radiation and substrate conditions but not the nature and the trends induced by the applied stimuli. By expanding the interatomic potential in a Taylor series around its equilibrium and considering the effective atomic z, we can derive the vibration frequency shift of the harmonic system[28,32,33]

$$\frac{1}{2}\mu(\Delta\omega)^2x^2 \cong \frac{1}{2}\frac{\partial u(r)}{\partial r^2}\bigg|_{r=d} x^2 \propto \frac{1}{2}\frac{E_z}{d^2}x^2.$$

As the first-order approximation, the lattice vibration frequency ω can be detected as Raman shift $\Delta\omega(z, d_z, E_z, \mu)$ from the reference point, $\omega(1, d_b, E_b, \mu)$, which depends functionally on the order z, length d_z, and energy E_z of the representative bond for the entire specimen (with z being involved[32]) and the reduced mass of the dimer atoms of the representative bond with $\mu = m_1m_2/(m_1 + m_2)$

$$\begin{aligned}\Delta\omega(z, d_z, E_z, \mu) &= \omega(z, d_z, E_z, \mu) - \omega(1, d_b, E_b, \mu),\\ &= \omega = \sqrt{\frac{d^2u(r)}{\mu dr^2}\bigg|_{r=d_z}} \propto \frac{z}{d_z}\left(\frac{E_z}{\mu}\right)^{1/2}. \quad (1)\end{aligned}$$

B. Size and temperature dependence

The BOLS theory[29] indicates that bonds between undercoordinated (z) atoms become shorter and stronger

$$\begin{cases} C_i(z_i) = d_i/d_0 = 2/\{1 + \exp[(12 - z_i)/8z_i]\} & (bond\ contraction)\\ C_i^{-m} = E_i/E_b & (bond\ strengthening)\end{cases}. \quad (2)$$

The index i is counted up to three from the outmost atomic layer inward as no atomic CN imperfection is justified at $i > 3$. The subscripts m and b denote the nature of the bond and in the bulk as a standard, for alloys and compounds m is four.[29] The bond contraction coefficient C_i varies only with the effective CN (or z) of the atom of concern regardless of the nature of the bond or the solid dimension. Fig. 1(a) illustrates schematically the BOLS correlation using the pairing atomic potential, $u(r)$. When the CN of an atom is reduced, the equilibrium atomic distance will contract from one unit (in d_0) to C_i, and the cohesive energy of the shortened bond will increase in magnitude from one unit (in E_b) to C_i^{-m}. The solid and the broken $u(r)$ curves correspond to the potentials of the pairing atoms with and without CN imperfection, respectively. The $u(r)$ curve slides towards shorter atomic distance along the C_i^{-m} line. Therefore, the CN imperfections of the nanostructures lead to the decrease of the average atomic cohesive energy, $E_B(0) = z_iE_i$, as observed from carbon allotropes.[34]

Taking the atomic coordination z and the temperature as the input parameters, the bond length and energy will change

$$\begin{cases} d(z,T) = d_b\left[(1 + (C_z - 1))\left(1 + \int_{T_0}^{T}\alpha(t)dt\right)\right]\\ E(z,T) = E_b\left[1 + \dfrac{(C_z^{-m} - 1) - \int_{T_0}^{T}\eta(t)dt}{E_b}\right]\end{cases}. \quad (3)$$

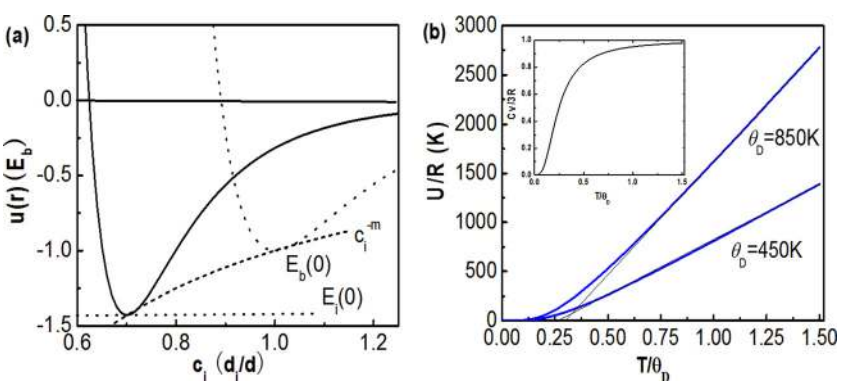

FIG. 1. (a) Atomic CN imperfection modified pairing potential energy. (b) Illustration of the temperature dependence of the reduced specific heat (inset) and its integration with respect to temperature (or the specific internal energy $U(T/\theta_D)$).

T_0 is the ambient reference temperature. For bulk material, the reduced mass μ and the z remain constant, and hence the Raman shift is proportional to the $E^{1/2}/d$ in dimension. The unknown $\omega(1)$ is the reference point from which the Raman shifts proceeds. The $\alpha(t)$ and $\eta(t)$ are the thermal expansion coefficient and the specific heat of the representative bond, respectively. These expressions indicate that heating will lengthen and weaken the bond while atomic CN reduction will shorten and strengthen the bond.

Combining Eqs. (1) and (3), we can formulate the size- and thermal-effect[35]

$$\frac{\omega(K,T)-\omega(1,T_0)}{\omega(z_b,T_0)-\omega(1,T_0)} \cong \begin{cases} (1+\Delta_R) & (\text{size}-\text{softening}) \\ (1-\Delta^T)^{1/2}\exp\left(\int_{T_0}^{T}\alpha dt\right) & (\text{themal}-\text{softening}) \end{cases}. \tag{4}$$

The size and thermally induced bond energy perturbation (Δ_R and $\Delta E^T=\Delta^T E_B$) follow the relationship

$$\begin{cases} \Delta_R=\sum\limits_{i\le 3}\gamma_i\left(\dfrac{\omega_i}{\omega_b}-1\right)=\sum\limits_{i\le 3}\gamma_i\left(\dfrac{z_i}{z_b}C_i^{-(m/2+1)}-1\right)<0 \\ \Delta^T=\dfrac{\int_0^T\eta(T/\theta_D)dt}{E_b}=\dfrac{\tau^2 R}{E_B}\left(\dfrac{T}{\theta_D}\right)^{\tau}\int_0^T\int_0^{\theta_D/T}\dfrac{x^{\tau+1}e^x}{(e^x-1)^2}dxdt \\ z_1=4(1-0.75/K),\quad \dfrac{\eta}{E_b}=\dfrac{C_V}{E_B} \\ \gamma_i=\dfrac{N_i}{N}=\dfrac{V_i}{V}\approx\dfrac{\tau C_i}{K},\quad (\tau=3) \end{cases}. \tag{5}$$

For a spherical dot, the $z_2=6$, and $z_3=12$.[36] γ_i is the portion of atoms in the ith atomic layer compared to the total number of atoms of the entire solid of different dimensionality ($\tau=1$, 2, and 3 correspond to a thin plate, a rod, and a spherical dot, respectively). $K=R/d$ is the number of atoms lined along the radius R of the nanosolid. The $\eta(T)=C_V/z$ is the specific heat per bond and ω_b (z_b, T_0) is the Raman shift of bulk at 0 K. The Δ^T is the integral of the specific heat reduced by the bond energy in three-dimensional Debye approximation (θ_D). When T is higher than θ_D, the three-dimensional specific heat (C_V) approaches a constant of 3R (R is the ideal gas constant). The $\omega(1)$, θ_D, and $E_B(0)$ are the uniquely adjustable parameters in calculating the Δ^T. From matching to the measurements we can quantify the aforementioned coefficients without involving hypothetic parameters or scattering processes.

III. RESULTS AND DISCUSSIONS

A. Size dependence

Considering the contribution from the outermost three atomic layers, a core-shell configuration is implemented. Generally, both theory and experimental results show that the size trend of a quantity Q(K) follows the linear dependence on the inverse of size 1/K, with K being the dimensionless form of size or the number of atoms lined along the radius of a sphere[30]

$$\omega(K)-\omega(\infty)=\begin{cases}\dfrac{-A}{K} & (\text{Measurement}) \\ \Delta_R(\omega(\infty)-\omega(1)) & (\text{Theory})\end{cases}. \tag{6}$$

Hence, the frequency shift from the dimer bond vibration to the bulk value, $\omega(\infty)-\omega(1)=-A/(\Delta_R K)$, is a constant as $\Delta_R\propto K$. As shown in Figs. 2(a) and 3(a), the BOLS predicting red shift of nanosolid CdS, CdSe, and Bi_2Se_3 are in good agreement with the experimentally measured results. Meanwhile, we can obtain the reference frequencies of these specimens, $\omega(1)=26.22$, 94.70, 106.57, 169.22 cm^{-1}. Taking $z_b=12$ for the bulk CdS, CdSe, and Bi_2Se_3, as a reference, the z-dependent frequency $\omega(z)$ for the possible Raman modes can be derived from Eq. (4)[28]

$$\begin{cases}\dfrac{\omega_x(z_i)-\omega_x(1)}{\omega_x(z_b)-\omega_x(1)}=\dfrac{zd(z_b)}{d(z_i)}\left(\dfrac{E_{zi}}{E_b}\right)^{1/2}=z_{ib}C_z^{-(m/2+1)} & (x=\mathrm{A}^1_{1g},\ \mathrm{E}^2_g,\ \text{and LO}) \\ \omega_x(z_i)=\omega_x(1)+[\omega_x(z_b)-\omega_x(1)]z_{ib}C_z^{-(m/2+1)}\end{cases}. \tag{7}$$

With the given peak values of the $A^1{}_{1g}$, $E^2{}_g$, and longitudinal optical (LO) modes of 72.5, 131.5, 300, and 212 cm^{-1} for the bulk CdS, CdSe, and Bi_2Se_3, the general expression for the z-dependent frequency can be derived

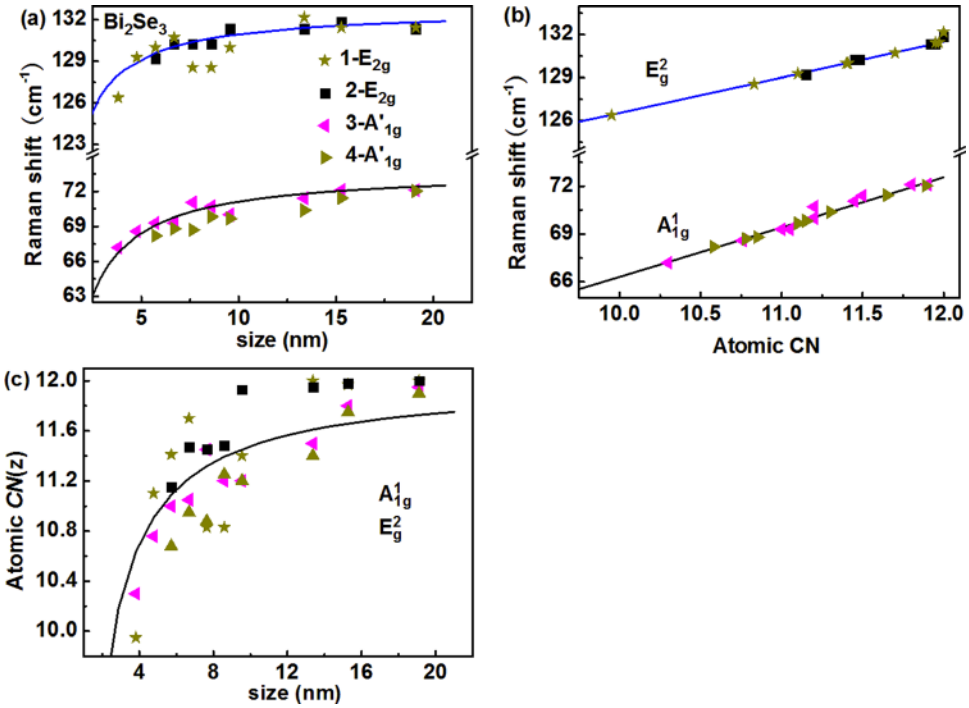

FIG. 2. (a) Comparison of the BOLS predictions with the theoretically calculated and the experimentally measured[14] red shift of Bi_2Se_3 phonons. (b) Theoretical reproduction of the CN-dependent Raman frequencies of the $A^1{}_{1g}/E^2{}_g$ modes. (c) Correlation functions of the atomic CN and the size for the Bi_2Se_3 $A^1{}_{1g}$ and $E^2{}_g$ modes.

$$\omega(z_i) = z_{ib} C_z^{-(m/2+1)} [\omega(z_b) - \omega(1)] + \omega(1)$$
$$= z_{ib} C_z^{-(m/2+1)} \times \begin{cases} 46.33 + 26.22 \ \ (Bi_2Se_3A^1_{1g}) \\ 36.80 + 94.70 \ \ (Bi_2Se_3E^2_g) \\ 193.43 + 106.57 \ (CdS) \\ 42.78 + 169.22 \ \ (CdSe) \end{cases} (cm^{-1}). \quad (8)$$

Therefore, we can reproduce the z-dependent $A^1{}_{1g}$ and $E^2{}_g$ modes of Bi_2Se_3 and the LO modes of CdS and CdSe with the derivative of the referential vibration frequencies using Eq. (8). Figs. 2(b) and 3(b) show the theoretical reproduction of the z-dependent Raman frequencies of the $A^1{}_{1g}$, $E^2{}_g$, and LO modes. In combination of Figs. 2(a) and 2(b), we can correlate the atomic CN and the particle size to obtain the relative change of bond length and bond energy,

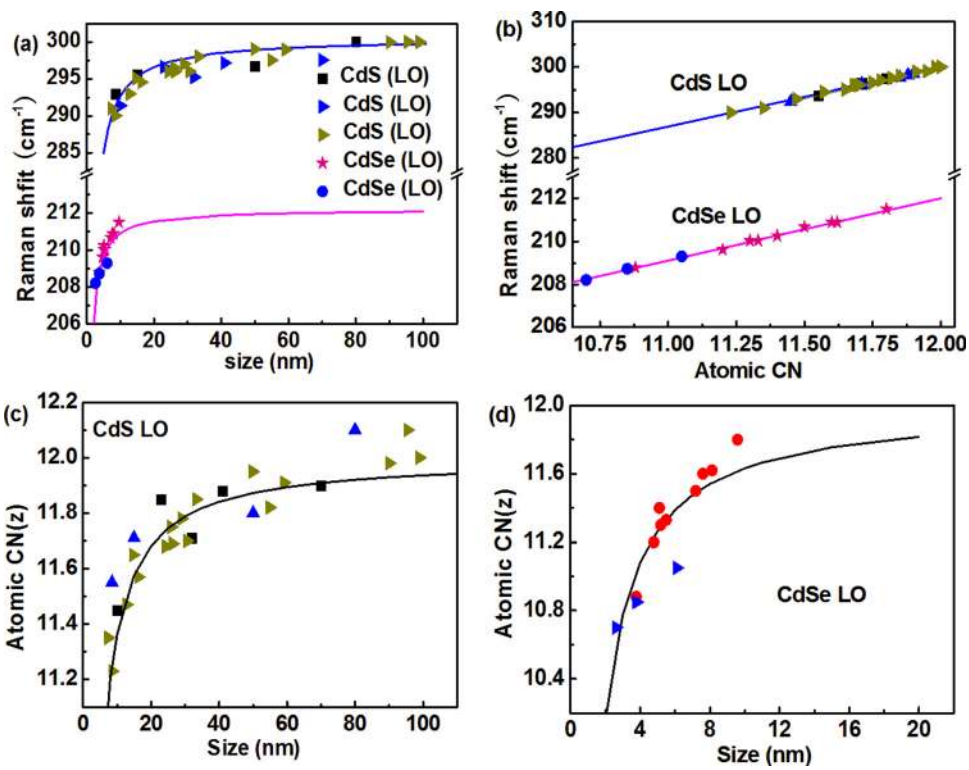

FIG. 3. (a) Comparison of the predictions with observations[11–13] on the size-dependent LO shifts of the nanosolid CdS and CdSe. (b) Theoretical reproduction of the CN-dependent Raman frequencies of LO mode. Panel (c) and the inset show the CN-size relationship for the LO mode.

as shown in Fig. 2(c). Using the same wise, the atomic CN-size relationship of CdS and CdSe can be obtained as shown in Fig. 3(c) and the inset. Based on Eqs. (1) and (2) and the BOLS derivative, $\langle CN(K)\rangle = 12[1+\sum_{i\le 3}\gamma_i(z_i/12-1)]$, we could reproduce the CN-size trend, shown in solid lines in Figs. 2(c) and 3(c).

B. Temperature dependence

Fig. 1(b) illustrates the temperature dependence of the reduced specific heat C_v (in units of gas constant R) and its integration with respect to the temperature T (or the termed specific internal energy), $U(T/\theta_D)$. At high T, especially when $T>\theta_D$, the integration of the specific heat or the specific internal energy depends linearly on T as shown in Fig. 1(b). At low temperatures, on the other hand, the integration shows a nonlinear relationship with respect to the temperature in a T^4 form. The range of nonlinearity depends highly on the Debye temperature θ_D, which can be seen from $U(T/\theta_D)$ in Fig. 1(b).

Like other V_2VI_3 compounds, Bi_2Se_3 and Sb_2Te_3 have 5 atoms in a rhombohedra unit cell, and four modes are Raman active, $2E_g+2A_{1g}$, with the frequencies in the 30–200 cm^{-1} range.[17,18] For the clarity and convenience, here we focus on the A_{1g} for Bi_2Se_3 and Sb_2Te_3 and the LO mode for CdS.

The fit of the frequency shift in the Raman spectrum was firstly conducted at $T>\theta_D$. Since the thermal expansion coefficient α is normally in a range of $10^{-6}\,K^{-1}\ll 1$. It is reasonable to ignore the thermal expansion for the first order approximation for $T>\theta_D$. Hence, Eq. (4) can be simplified as

$$\omega(z_b,T)\cong\omega(z_b,T_0)-[\omega(z_b,T_0)-\omega(1,T_0)]\times\frac{\eta}{2E_b(0)}T,$$
$$\cong\omega(z_b,T_0)-[\omega(z_b,T_0)-\omega(1,T_0)]\times B_{exp}T. \quad (9)$$

When the reference frequency is unknown, experimental slope $B=[\omega(z_b,T_0)-\omega(1,T_0)]B_{exp}$ and the $E_b(0)\cong[\omega(z_b,T_0)-\omega(1,T_0)]\times 1/2\times\eta/B$. By matching theory with the parameters of $E_B(\omega)$, $\alpha(t)$,[37,38] and θ_D[39–41] to the measured T-dependent Raman shift of CdS, Bi_2Se_3, and Sb_2Te_3, as shown in Fig. 2, the reference frequencies were calculated as 106.57 cm^{-1}, 40.57 cm^{-1}, and 30.25 cm^{-1}, respectively. Then, from the relation of $B_{exp}\cong 1/2\times\eta/E_b(0)$ with $\eta_1=3R/z$ $(T>\theta_D)$, the cohesive energy E_B of Bi_2Se_3, Sb_2Te_3, CdS bulk, and CdS nanostructures can be estimated as 1.24, 1.09, 2.13, and 1.72 eV/atom, respectively, as listed in Table I. The atomic CN imperfection of the nanostructures leads to the decrease of the average atomic cohesive energy, according to BOLS theory; therefore the CdS bulk E_B is higher than nanostructures. Fig. 4(a) shows the thermal softening of CdS phonons.

Matching to the measured T-dependent Raman shift of CdS, Bi_2Se_3, and Sb_2Te_3, as shown in Figs. 4(a) and 4(b), turns out the Debye temperature, reference frequencies, and the atomic cohesive energy. At $T\sim\theta_D/3$, the Raman shift turns gradually from the nonlinear to the linear form when the temperature is increased. The slow decrease of the Raman shift at very low temperatures arises from the small $\int_0^T\eta dt$ values as the specific heat $\eta(t)$ is proportional to T^3 for the three-dimensional system at very low temperatures. These results imply that the Debye temperature determines

TABLE I. Quantity information of atomic cohesive energy (E_B), Debye temperature (θ_D), and reference frequencies ($\omega(1)$) derived from the reproduction of the T-dependent Raman shift of Bi_2Se_3, Sb_2Te_3, and CdS bulk and nanostructures.

					θ_D (K)	
	Raman mode	E_B (eV)	$\omega(1)$ (cm^{-1})	B_{exp} (cm^{-1}/K)	Output	Reference
CdS (bulk)	LO	2.13	106.57	0.012[a]	450	460[b]
CdS (nano)	LO	1.72	106.57	0.015[a]	300	300[b]
Sb_2Te_3	A_{1g}^2	1.09	30.65	0.018[c]	165	162[d]
Bi_2Se_3	A_{1g}^2	1.24	40.57	0.015[c]	185	182[e]

[a]Reference 16.
[b]Reference 41.
[c]Reference 15.
[d]Reference 40.
[e]Reference 39.

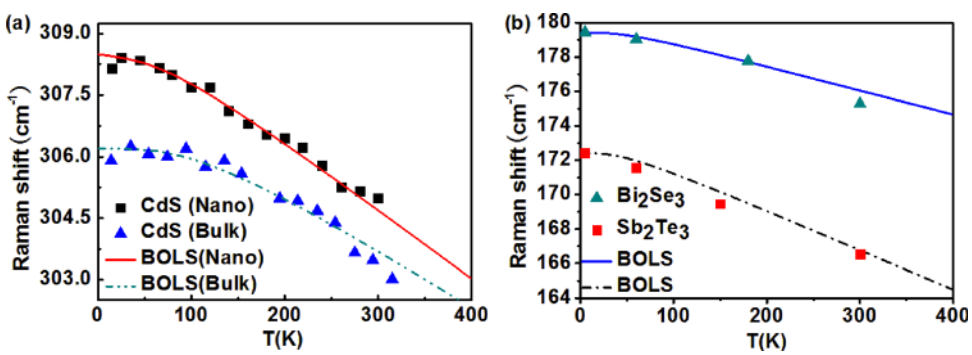

FIG. 4. BOLS reproduction of the measured T-dependent Raman shifts of (a) CdS bulk and nanostructures [Ref. 16], (b) Bi_2Se_3 and Sb_2Te_3 [Ref. 15] with derived information as given in Table I.

the width of the shoulder. In Fig. 4(a), the Debye temperature of CdS bulk is higher than CdS nanostructures, and hence the linearity of the optical frequency shift in the Raman spectrum for CdS bulk extends to higher temperature; the slope of $\Delta\omega$-T for CdS nanostructures is greater than that of CdS bulk because the average atomic cohesive energy of CdS nanostructure is smaller, which is the thermal softening of CdS Raman shift respond to different atomic cohesive energy. The inverse cohesive energy, $1/E_B(0)$, determines the slope at high temperatures in the T-dependent Raman shift curve.

IV. CONCLUSION

From the perspectives of BOLS correlation, core-shell configuration, and LBA approach, we have been able to clarify, formulate, and correlate the size and thermal softening of the Raman phonons of CdS, CdSe, Bi_2Se_3, and Sb_2Te_3 without involvement of the mode Grüneisen parameters or the multi-phonon resonant scattering or decay. Quantitative information of atomic cohesive energy, the reference frequencies, and Debye temperature in each case has been obtained, which is beyond the scope of conventional approaches. Agreement between the calculation and experimental data may demonstrate that not only the current expression could represent the true situation of the thermally driven optical phonon frequency red-shift in the Raman spectrum but also the enhanced power of the Raman spectroscopy in quantifying the information.

ACKNOWLEDGMENTS

Financial supports from NSF (Nos. 11172254 and 11002121) China Postdoctoral Foundation (No. 2012M511738), SRFDP (20104301120005), and HPIFP (CX2011B259) of China are gratefully acknowledged.

C.Q. is associated with honorary appointment at 1 and 3.

[1]J. Chen, H. J. Qin, F. Yang, J. Liu, T. Guan, F. M. Qu, G. H. Zhang, J. R. Shi, X. C. Xie, C. L. Yang, K. H. Wu, Y. Q. Li, and L. Lu, Phys. Rev. Lett. **105**, 176602 (2010).
[2]H. Steinberg, D. R. Gardner, Y. S. Lee, and P. Jarillo-Herrero, Nano Lett. **10**, 5032 (2010).
[3]J. G. Checkelsky, Y. S. Hor, R. J. Cava, and N. P. Ong, Phys. Rev. Lett. **106**, 196801 (2011).
[4]X. Zhang, J. Wang, and S.-C. Zhang, Phys. Rev. B **82**, 245107 (2010).
[5]R. V. Aguilar, A. V. Stier, W. Liu, L. S. Bilbro, D. K. George, N. Bansal, L. Wu, J. Cerne, A. G. Markelz, S. Oh, and N. P. Armitage, Phys. Rev. Lett. **108**, 087403 (2012).
[6]X. L. Qi, T. L. Hughes, and S.-C. Zhang, Phys. Rev. B **78**, 195424 (2008).
[7]A. M. Essin, J. E. Moore, and D. Vanderbilt, Phys. Rev. Lett. **103**, 259902 (2009).
[8]A. W. Schill and M. A. El-Sayed, J. Phys. Chem. B **108**, 13619 (2004).
[9]S. R. Park, W. S. Jung, C. Kim, D. J. Song, C. Kim, S. Kimura, K. D. Lee, and N. Hur, Phys. Rev. B **81**, 041405 (2010).
[10]H. Borchert, D. Dorfs, C. McGinley, S. Adam, T. Möller, H. Weller, and A. Eychmüller, J. Phys. Chem. B **107**, 7486 (2003).
[11]D. S. Chuu and C. M. Dai, Phys. Rev. B **45**, 11805 (1992).
[12]A. Tanaka, S. Onari, and T. Arai, Phys. Rev. B **45**, 6587 (1992).
[13]Y. N. Hwang, S. H. Park, and D. Kim, Phys. Rev. B **59**, 7285 (1999).
[14]J. Zhang, Z. Peng, A. Soni, Y. Zhao, Y. Xiong, B. Peng, J. Wang, M. S. Dresselhaus, and Q. Xiong, Nano Lett. **11**, 2407 (2011).
[15]Y. Kim, X. Chen, Z. Wang, J. Shi, I. Miotkowski, Y. P. Chen, P. A. Sharma, A. L. L. Sharma, M. A. Hekmaty, Z. Jiang, and D. Smirnov, Appl. Phys. Lett. **100**, 071907 (2012).
[16]E. S. F. Neto, N. O. Dantas, S. W. d. Silva, P. C. Morais, M. A. P. d. Silva, A. J. D. Moreno, V. L. Richard, G. E. Marques, and C. T. Giner, Nanotechnology **23**, 125701 (2012).
[17]W. Richter and C. R. Becker, Phys. Status Solidi B **84**, 619 (1977).
[18]W. Richter, A. Krost, U. Nowak, and E. Anastassakis, Z. Phys. B: Condens. Matter **49**, 191 (1982).
[19]A. Dieguez, A. Romano-Rodriguez, A. Vila, and J. R. Morante, J. Appl. Phys. **90**, 1550 (2001).
[20]Y. I. Yuzyuk, R. S. Katiyar, V. A. Alyoshin, I. N. Zakharchenko, D. A. Markov, and E. V. Sviridov, Phys. Rev. B **68**, 104104 (2003).
[21]P. S. Dobal, S. Bhaskar, S. B. Majumder, and R. S. Katiyar, J. Appl. Phys. **86**, 828 (1999).
[22]Z. Iqbal and S. Veprek, J. Phys. C: Solid State Phys. **15**, 377 (1982).
[23]H. Richter, Z. P. Wang, and L. Ley, Solid State Commun. **39**, 625 (1981).
[24]I. H. Campbell and P. M. Fauchet, Solid State Commun. **58**, 739 (1986).
[25]N. Ohtani and K. Kawamura, Solid State Commun. **75**, 711 (1990).
[26]T. M. G. Mohiuddin, A. Lombardo, R. R. Nair, A. Bonetti, G. Savini, R. Jalil, N. Bonini, D. M. Basko, C. Galiotis, N. Marzari, K. S. Novoselov, A. K. Geim, and A. C. Ferrari, Phys. Rev. B **79**, 205433 (2009).
[27]M. X. Gu, L. K. Pan, B. K. Tay, and C. Q. Sun, J. Raman Spec. **38**(6), 780–788 (2007).
[28]X. X. Yang, J. W. Li, Z. F. Zhou, Y. Wang, L. W. Yang, W. T. Zheng, and C. Q. Sun, Nanoscale **4**, 502 (2012).
[29]J. W. Li, L. W. Yang, Z. F. Zhou, X. J. Liu, G. F. Xie, Y. Pan, and C. Q. Sun, J. Phys. Chem. B **114**(4), 1648–1651 (2010).
[30]C. Q. Sun, Prog. Mater. Sci. **54**, 179 (2009).
[31]W. G. Han and C. T. Zhang, J. Phys.: Condens. Matter **3**, 27 (1991).
[32]C. Q. Sun, Prog. Solid State Chem. **35**, 1 (2007).
[33]J. Li, S. Ma, X. Liu, Z. Zhou, and C. Q. Sun, Chem. Rev. **112**, 2833 (2012).
[34]Y. Wang, X. X. Yang, J. W. Li, Z. F. Zhou, W. T. Zheng, and C. Q. Sun, Appl. Phys. Lett. **99**, 163109 (2011).
[35]X. X. Yang, J. W. Li, Z. F. Zhou, Y. Wang, W. T. Zheng, and C. Q. Sun, Appl. Phys. Lett. **99**, 133108 (2011).
[36]C. Q. Sun, L. K. Pan, C. M. Li, and S. Li, Phys. Rev. B **72**, 134301 (2005).
[37]P. V. B. Lakshmi and K. Ramachandran, Cryst. Res. Technol. **41**, 498 (2006).
[38]X. Chen, H. D. Zhou, A. Kiswandhi, I. Miotkowski, Y. P. Chen, P. A. Sharma, A. L. L. Sharma, M. A. Hekmaty, D. Smirnov, and Z. Jiang, Appl. Phys. Lett. **99**, 261912 (2011).
[39]G. E. Shoemake, J. A. Rayne, and R. W. J. Ure, Phys. Rev. **185**, 1046 (1969).
[40]J. S. Dyck, W. Chen, C. Uher, Č. Drašar, and P. Lošt'ák, Phys. Rev. B **66**, 125206 (2002).
[41]J. Rockenberger, L. Tröger, A. Kornowski, T. Vossmeyer, A. Eychmüller, J. Feldhaus, and H. Weller, J. Phys. Chem. B **101**, 2691 (1997).